energy&fuels

Article

pubs.acs.org/EF

Shock-Tube Experiments and Kinetic Modeling of 2-Methylfuran Ignition at Elevated Pressure

Liangjie Wei, Chenglong Tang,* Xingjia Man, and Zuohua Huang*

State Key Laboratory of Multiphase Flow in Power Engineering, Xi'an Jiaotong University, Xi'an, Shaanxi 710049, People's Republic of China

Supporting Information

ABSTRACT: Ignition delays of 2-methylfuran were measured behind reflected shock waves over a wide range of experimental conditions: equivalence ratios from 0.25 to 2.0, average pressures from 1.25 to 10.65 bar, temperatures from 1120 to 1700 K, and oxygen concentrations up to 20%. Results show that the ignition delay decreases with increasing the pressure and decreasing the dilution ratio. For a given dilution ratio, there exists a crossover in the ignition delay time dependence upon the equivalence ratio and the crossing point shifts to the higher temperature at a higher pressure. The measured ignition delays of 2-methylfuran show good agreement with the previous data at atmospheric pressure. The 2-methylfuran model NUI_MF2 well predicts the ignition delays of 2-methylfuran at 1.25 bar but gives the underprediction when pressures are elevated to 4.25 and 10.65 bar. Sensitivity analysis identifies the importance of the reactions involving the *n*-butadienyl radical (C_4H_5-*n*) in the ignition process of 2-methylfuran. Better prediction on ignition delay times is achieved by perturbing the rate constants of *β*-scission reactions for the C_4H_5-*n* radical, and these perturbations do not affect the primary fuel consumption flux based on the reaction pathway analysis.

1. INTRODUCTION

Following the substantial development and utilization of the biofuels, such as alcohols, ethers, and methyl esters,[1,2] there now exists considerable interests in the second-generation biofuels, such as furan and its derivatives, 2-methylfuran (2-MF) and 2,5-dimethylfuran (25-DMF). These so-called furans belong to the unsaturated cyclic ether family, can be produced from non-food biomass, such as stalks and leaves,[3,4] and does not threaten food supply and biodiversity. In comparison to ethanol, 2-MF and 25-DMF are water-insoluble and have better thermal or physical properties, such as higher energy density and octane number. All of these attributes render them more promising as gasoline substitutes.[3]

Lifshitz et al.[5] studied the thermal decomposition of 25-DMF behind reflected shock waves of temperatures from 1070 to 1370 K and pressures from 2.1 to 2.7 bar. They observed the production of 2-MF in the decomposition of 25-DMF by elimination of methyl on the furan ring. Similarly, Wu et al.[6] examined the combustion intermediates of 2,5-methylfuran in a low-pressure premixed laminar flame and found the presence of 2-MF in the 25-DMF flame. Thus, 2-MF is a product in either pyrolysis or oxidation of 25-DMF. Recently, Friese et al.[7] and Sirjean et al.[8] studied the reactions between 25-DMF and H atoms by experiment and numerical calculation, respectively, and they both found that ipso substitution 25-DMF + H → 2-MF + CH_3 is the major pathway. Consequently, 2-MF, as a biofuel candidate, needs a better understanding of its kinetic mechanism for its further applications.

In terms of previous contributions for 2-MF, Thewes et al.[9] studied the performance of 2-MF in a direct-injection spark-ignition (DISI) single-cylinder engine and observed good combustion stability during engine cold start. Ohtomo et al.[10] reported the autoignition characteristics of furans and other biofuels in a rapid compression machine and found that 2-MF has comparable knock inhibition capability to ethanol. Wang et al.[11] compared the combustion and emissions of 2-MF to gasoline, ethanol, and 25-DMF in a single-cylinder spray-guided DISI engine, and the results showed that 2-MF gives higher indicated efficiency and lower aldehyde emissions compared to those of gasoline. Meanwhile, fundamental studies on 2-MF were extensively conducted for the understanding of combustion chemistry and development of the associated kinetic mechanisms. Specifically, Grela et al.[12] and Lifshitz et al.[5,13,14] studied the thermal decomposition of furan and its derivatives (2-MF and 25-DMF). Their results showed that 25-DMF has the highest overall reactivity, followed by 2-MF, with furan being the least reactive. Somers et al.[15] measured the ignition delays and laminar flame speeds of 2-MF at atmospheric pressure and developed a 2-MF kinetic model (hereafter called NUI_MF2). The model prediction is in reasonable agreement with the measured ignition delays, laminar flame speeds, and thermal decomposition results in ref 14. Wei et al.[16] identified the primary intermediates in a low-pressure premixed laminar flame of 2-MF using tunable synchrotron vacuum ultraviolet photoionization and molecular beam mass spectrometry and also provided the possible reaction pathway of 2-MF. Recently, Tran et al.[17] investigated mole fraction of products in the 2-MF low-pressure laminar flame by electron-ionization molecular-beam mass spectrometry (EI–MBMS) and gas chromatography (GC). A comprehensive combustion chemistry model was constructed and validated against the mole fraction of products in furan, 2-MF, and 25-DMF flame under low-pressure conditions. Together with chemistry kinetic simulation, the main reaction pathways of 2-MF are identified.

Received: September 9, 2013
Revised: November 5, 2013
Published: November 6, 2013

Even though the understanding on 2-MF combustion is still limited, especially at the elevated pressure condition, further study on it is necessary. Thus, the objectives of this study are to acquire the ignition delays of 2-MF at elevated pressures and identify the important role of pressure in terms of the kinetic mechanisms and applications. A comparison on the measured ignition delays of 2-MF and predictions with an available kinetic model are made to evaluate model performance. Sensitivity and reaction pathway analyses are employed to identify the important reactions in the ignition process of 2-MF at elevated pressure.

2. EXPERIMENT AND MODELING APPROACHES

The shock-tube facility employed for the ignition delay measurement was described in the previous publication.[18] Briefly, the helium-driven, unheated, shock tube consists of a 2 m long driver section and a 7.3 m long driven section with a diameter of 11.5 cm. Prior to each experiment, the entire tube was evacuated to a pressure below 10^{-4} Torr. Four equally spaced (300 mm), fast-response sidewall pressure transducers (PCB 113B26) are located along the end part of the driven section. The endwall pressure and CH* emission signal are detected by an endwall pressure transducer (PCB 113B03) and photomultiplier (Hamamatsu CR 131) with a 430 ± 10 nm filter, respectively. All of the pressure transducers are shielded with silicone rubber to minimize heat transfer. Three time-counters (Fluke PM 6690) are used to measure the time intervals between the instants of shock arrival at each pressure transducer location, with which the shock velocity at the endwall is determined by linearly extrapolating the axial velocity profile to the endwall. Typical attenuation rates of incident shock are less than 3%. The conditions behind the reflected shock wave are calculated by the chemical equilibrium program GasEq,[19] assuming frozen chemistry, with the thermodynamic data of 2-MF calculated by Somers et al.[15] The uncertainties of the temperature behind the reflected shock wave and the measured ignition delays are less than 25 K and 15%, respectively.

The ignition delay is determined as the time interval between the arrival of the incident shock and the onset of ignition at the endwall. As shown in Figure 1, the arrival of the incident shock is evidenced by the

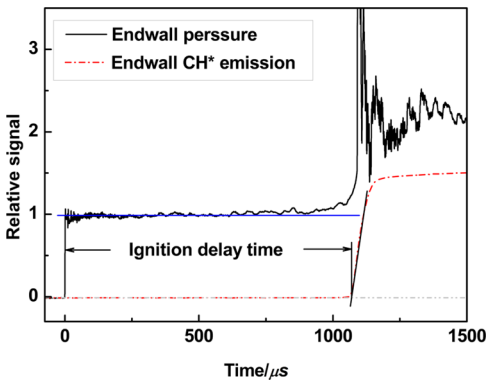

Figure 1. Determination of the ignition delay time for 2-MF.

first steep rise on the endwall pressure profile. The ignition is evidenced by the pressure spike behind the reflected shock and the simultaneously observed steep increase of the CH* emission. Consequently, the onset of ignition is defined by extrapolating the maximum slope line of either the CH* profile or the endwall pressure profile to the baseline. In the current study, the CH* definition and the pressure definition give similar ignition delay times, with a typical relative difference less than 3%.

Mixtures of 2-MF (99% in purity) and high-purity oxygen and argon (>99.995%) were prepared in a 128 L stainless tank, allowing for sufficient mixing time before experiment. For all test conditions, the partial pressure of the fuel was assured to be less than $^1/_3$ of its saturated vapor pressure at the tank temperature to exclude fuel condensation. Compositions of all mixtures are given in Table 1, in which φ is the equivalence ratio and D is the dilution ratio (X_{Ar}/X_{O_2}).

Table 1. Gas Composition of 2-MF/O_2/Ar Mixtures in This Study

fuel	mixture	ϕ	D	fuel (%)	O_2 (%)	Ar (%)
2-MF	1	1.0	21	0.752	4.511	94.737
	2	2.0	15.5	1.980	5.941	92.079
	3	1.0	15.5	1.000	6.000	93.000
	4	0.5	15.5	0.503	6.030	93.467
	5	0.25	15.5	0.252	6.045	93.703
	6	1.0	9.9	1.506	9.036	89.448
	7	1.0	3.76	3.383	20.298	76.319

For the calculation of ignition delays of 2-MF, we shall use the detailed kinetic model (NUI_MF2) of Somers et al.,[15] which incorporates the submechanisms of furan[20,21] and aromatics[22] and has been validated against the ignition delays and laminar flame speeds at atmosphere pressure as well as the thermal decomposition results of Lifshitz et al.[14]

Simulation on ignition delay times were performed through the constant volume homogeneous reactor in Chemkin II,[23,24] assuming a zero-dimensional and constant volume adiabatic model. It is noted that, in the model of NUI_MF2, some of the pressure dependence reactions are given in PLOG formulation, which is not a formal rate constant expression in Chemkin II. However, a PLOG formulation replacement tool was developed by the Curran group. Thus, by the help of this tool, NUI_MF2 can be specified to any desired pressure and be used in modeling by Chemkin II. In modeling the ignition, the point of maximum rate of pressure rise (maximum dp/dt point) is chosen as the state of ignition. With regard to the pressure rise before ignition caused by the non-ideal effect being much smaller (see Figure 1) and most of the measured ignition delay times being less than 2 ms, a non-ideal effect is not considered in the ignition calculation.

3. RESULTS AND DISCUSSION

3.1. Comparison to a Previous Study. As discussed above, few studies report the ignition delays measurements on 2-MF. Somers et al.[15] conducted an experiment on 2-MF ignition delays on a shock tube in a fuel fraction of 1% at atmospheric pressure. However, the average pressure range in this work is from 1.25 to 10.65 bar. For a rigorous comparison, the data of mixture 3 (1% 2-MF/6% O_2/93% argon; ϕ = 1.0; D = 15.5; and the same gas composition as that of Somers et al.[15]) was correlated in an Arrhenius form through the multi-regression analysis method, as shown in eq 1. Then, the data of mixture 3 at 1.25 bar are scaled to 1.0 atm through eq 2. Figure 2 compares the measured ignition delays of mixture 3 to those from Somers et al.[15] as well as the calculated values using the NUI_MF2 model, at a pressure of 1.0 atm. A comparison shows good agreement among the present measurements, the measurements of Somers et al.,[15] and the numerical predictions using NUI_MF2. This agreement from different sources confirms the accuracy in the measurement of ignition delays using the shock-tube facility

$$\tau = 4.35 \times 10^{-3} p^{-0.662} \exp(16290/T) \quad (1)$$

where τ is the ignition delay time in μs, p is the pressure in atm, and T is the temperature in K.

$$\tau_{cor} = \tau_{exp}\left(\frac{P_{cor}}{P_{exp}}\right)^{-0.662} \quad (2)$$

3.2. Effect of the Pressure. Ignition delays of mixture 3 at an elevated pressure are presented in Figure 3. As expected, the

dx.doi.org/10.1021/ef401809y | Energy Fuels 2013, 27, 7809−7816

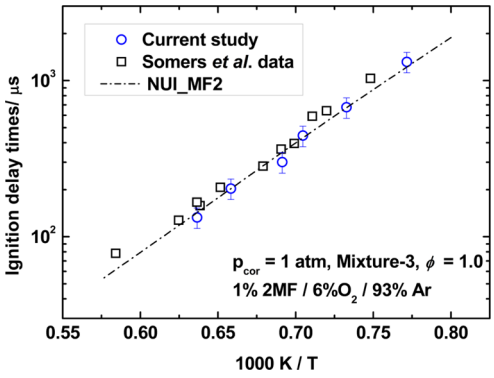

Figure 2. Comparison of the measured ignition delay times in the current study to the data of Somers et al.[15] and model predictions at a normalized pressure of 1.0 atm.

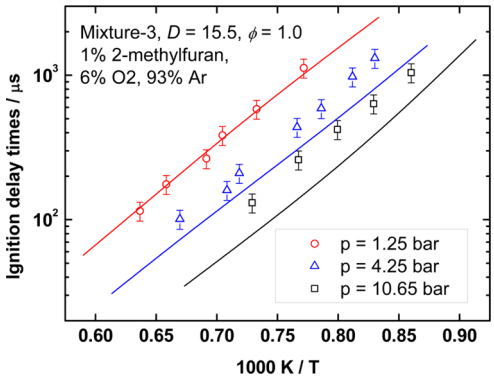

Figure 3. Effects of the pressure on ignition delay times of 2-MF for 1% 2-MF, 6% oxygen, and 93% argon (mixture 3; D = 15.5; and ϕ = 1.0). Symbold, measurements; solid lines, NUI_MF2.

ignition delay decreases with increasing the pressure. This trend can also be evidenced by the pressure exponent α in eq 1, with a negative value for mixture 3. The calculated results show good agreement with the measurements at 1.25 bar, although they become consistently lower for higher pressures. The raw data for other mixtures (providing in the Supporting Information) show a similar dependence upon pressure. However, when the pressure is increased, the NUI_MF2 model underpredicts the measured ignition delays, although both the measurements and prediction show a similar overall activation energy.

3.3. Effect of the Dilution Ratio. The effect of the dilution ratio (D) on the ignition delays of 2-MF was studied at elevated pressures. Figure 4a shows the ignition delays of mixtures 1, 3, 6, and 7 (D = 21, 15.5, 9.9, and 3.76, respectively) at an average pressure of 1.25 bar under stoichiometric conditions. Results show that ignition delay increases with an increasing dilution ratio (argon concentration). This is reasonable because, for a given equivalence ratio, an increase in the dilution ratio reduces the concentrations of both fuel and oxidizer, leading to the reduced overall reactivity. The calculated ignition delays agree well with the measurements for mixture 1 (D = 21.0) and mixture 3 D = 15.5), while the simulation yields slightly lower values for mixture 6 (D = 9.9) and mixture 7 (D = 3.76), especially under a relatively lower temperature range.

At elevated pressures, as shown in panels b and c of Figure 4, the NUI_MF2 model prediction yields fair agreement with the measurements, with 34 and 43% lower predictions than the measurements at 4.25 and 10.65 bar, respectively, for mixture 3 at

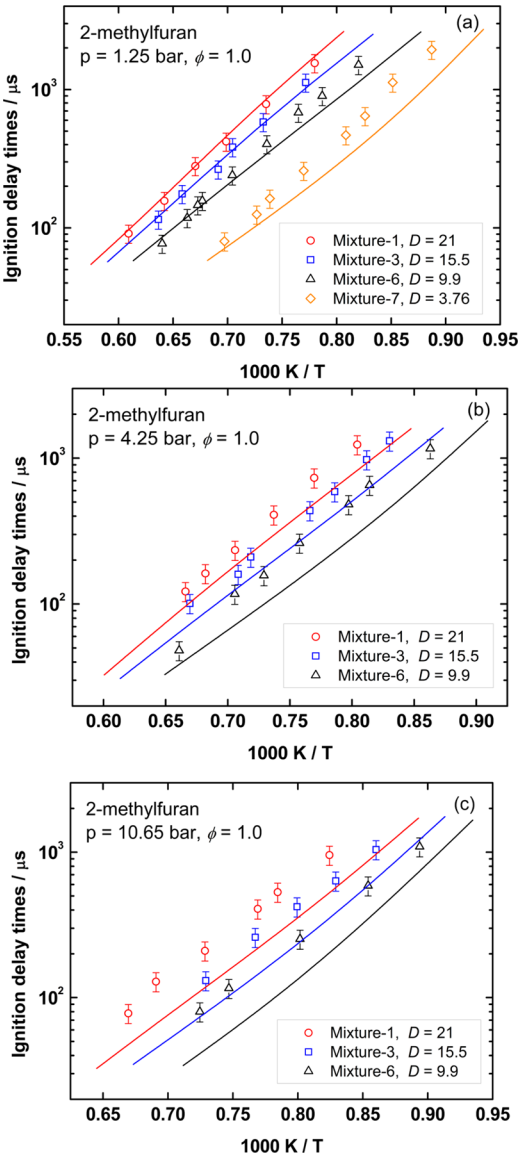

Figure 4. Effects of the dilution ratio on ignition delay times of 2-MF at different pressures. Symbols, measurements; lines, NUI_MF2 model predictions.

1250 K. Because the NUI_MF2 model was only validated against experimental data at atmospheric pressure, it may not capture the 2-MF ignition behaviors at elevated pressure.

3.4. Effect of the Equivalence Ratio. Figure 5 shows the effect of the equivalence ratio by comparing the ignition delays of mixtures 2, 3, and 5 (ϕ = 2.0, 1.0, and 0.25, respectively) at a fixed dilution ratio of 15.5. At a pressure of 1.25 bar, as shown in Figure 5a. Both the experimental and calculated values exhibit an increasing trend of the ignition delays with an increasing equivalence ratio, indicating that fuel-lean mixtures are more reactive. Healy et al.[25] also observed a similar trend for butane at low pressure and relatively high temperature conditions. They attributed it to the dominance of the chain-branching reaction, H + O_2 → O + OH, in this temperature range and, hence, the corresponding reactivity with an increasing equivalence ratio. It is noted that the difference in the O_2 concentration is very small for mixtures 2, 3, and 5, as shown in Table 1. The fuel concentration increases significantly with an increasing equivalence ratio, leading to the increased fuel scavenging of the H radicals through

dx.doi.org/10.1021/ef401809y | Energy Fuels 2013, 27, 7809−7816

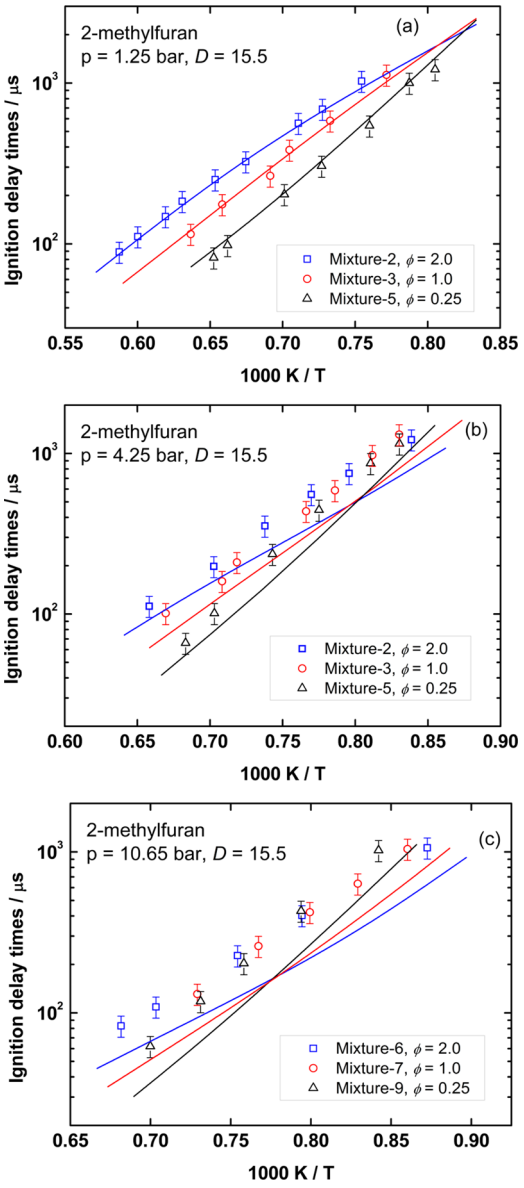

Figure 5. Effects of the equivalence ratio on ignition delay times for 2-MF at different pressures. Symbols, measurements; lines, NUI_MF2 model predictions.

fuel + H → R + H_2 (where R is the fuel radical; reaction pathway analysis shows that ⬠ + H → ⬠ + H_2 is the most prominent reaction) and consequently reduction of the overall reactivity. However, the difference in ignition delay among three mixtures tends to vanish gradually as the temperature decreases to 1210 K, indicating that there must be a crossing point at about 1210 K, and the dependence of the ignition delay upon the equivalence ratio will reverse when the temperature is further decreased.

At a pressure of 4.25 bar in Figure 5b, a crossing point at about 1250 K is indeed observed when the temperature shifts to the lower range. In particular, when the temperature is lower than 1250 K, ignition delay exhibits a weak negative dependence upon the equivalence ratio. This behavior is consistent with the observation of Healy et al.[25,26] for butane isomers and from Stranic et al.[27] for *n*-butanol. This weak negative dependence at a relatively lower temperature is caused by the increased radical production through the chain-branching reaction, fuel + HO_2 → R + H_2O_2, followed by the reaction H_2O_2 + M → OH + OH + M. When the pressure further increases to 10.65 bar, as shown in Figure 6c, the crossing point temperature increases to about 1290

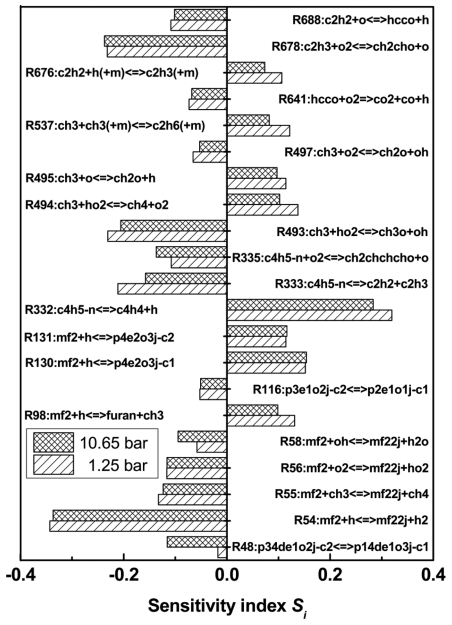

Figure 6. Sensitivity analysis for 1% 2-MF, 6% O_2, and 93% argon mixture (mixture 3; D = 15.5; and ϕ = 1.0) at 1330 K (reaction R349, H + O_2 → O + OH, is the most sensitivity reaction and is not given here to highlight the sensitivities for other reactions).

K, indicating that the three-body reaction, H + O_2 + M → HO_2 + M, is favorable over the branching reaction, H + O_2 → OH + H, as pressure is increased. The NUI_MF2 model can capture this trend, although it underpredicts the ignition delays at elevated pressure.

3.5. Sensitivity Analysis. Because the NUI_MF2 model yields fairly good comparisons to the measured ignition delays of 2-MF at atmospheric pressure but underpredicts at elevated pressure, it is of interest to examine the important reactions at elevated pressures for 2-MF. Sensitivity analysis was performed to identify the dominant reactions, especially pressure dependence reactions, for the predictions with pressure variation using the NUI_MF2 model. The sensitivity index is calculated by perturbing the reaction rate as

$$S_i = \frac{\log_{10}(\tau_{2k}/\tau_{0.5k})}{\log_{10}(2/0.5)} \quad (3)$$

where τ is the ignition delay. A negative sensitivity indicates an increase in the rate of the ith reaction and leads to a reduced ignition delay and an increased overall reactivity.

Figure 6 yields the most sensitive reactions for mixture 3 at 1330 K and pressures of 1.25 and 10.65 bar. Except for reaction R48, all reactions yield similar sensitivity indexes at pressures of 1.25 and 10.65 bar. H-abstraction reactions by small species (H, OH, CH_3, and O_2) attacking the methyl side of fuel play the promoting role in the model. Meanwhile, reaction R98 consumes the H radical and forms a less reactive methyl radical, and the furan molecular inhibits the system reactivity. Moreover, reactions R332, R333, and R335 involving the *n*-butadienyl radical (C_4H_5-*n*, C═C−C═C*) yield relatively large sensitivity indexes. The rest of the sensitive reactions all involve small radicals. The termination reactions R494 and R537 play an inhibition role on the reactivity. Generally, reactions R54 and

dx.doi.org/10.1021/ef401809y | *Energy Fuels* 2013, 27, 7809−7816

R332 are the two most sensitive reactions. Reaction R54, with a rate of $k_{54} = 3.78 \times 10^6 T^{2.4} \exp(-2370/T)$, is calculated on the basis of CBS-QB3 energetics and partition functions and achieves better agreement with a laminar flame speed of 2-MF.[15] Considering the relatively large sensitivity index at both pressures, a perturbation on the rate of reaction R54 will affect the prediction on the ignition delays at all pressure ranges. Moreover, reaction R54 is a bimolecular reaction, which does not show any pressure dependence behavior. Thus, any modifications on the rate coefficient of reaction R54 are not justified.

With regard to β-scission reaction R332 (C_4H_5-$n \rightarrow C_4H_4 + H$), a unimolecular decomposition reaction exhibits the pressure dependence behavior and shows the largest positive sensitivity index under the investigated conditions. It competes with another β-scission reaction R333 (C_4H_5-$n \rightarrow C_2H_2 + C_2H_3$) in C_4H_5-n consumption on the basis of the integration reaction flux analysis in Figure 7. In the NUI_MF2 model, the C_4H_5-n radical

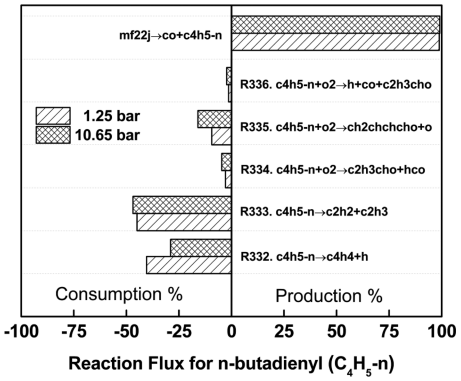

Figure 7. Integration reaction flux analysis for the *n*-butadienyl radical (C_4H_5-n) at 1330 K for mixture 3.

is mostly produced from fuel radical mf22j (⌓), which is a radical formed by H-abstraction reactions of 2-MF at the methyl side. As reported by Somers et al.,[15] under the shock-tube high-temperature conditions, 39.9 and 33.1% of 2-MF undergo H-abstraction reactions for the fuel-lean and -rich mixtures, respectively. Thus, it is reasonable that the reactions involving the C_4H_5-n radical show a large sensitivity on ignition of 2-MF because a large fraction of 2-MF will ultimately convert to it. Also, as indicated in Figure 7, the consumption of C_4H_5-n undergoing reaction R333 is the largest channel and increases with the increase of the pressure. However, as pointed out by Law,[28] the β C−H bond energy (35 kcal mol^{-1}) is weaker than the β C−C bond (41 kcal mol^{-1}) on the C_4H_5-n radical; thus, the probable products of C_4H_5-n through the β-scission are C_4H_4 (vinyl acetylene) and a H atom. However, the β-scission reactions involving C_4H_5-n in the NUI_MF2 model do not capture this behavior.

As shown in Figure 6, reaction R332 is an inhibition reaction, whereas reaction R333 is a promotion reaction. Therefore, it is suggested that the underprediction of ignition delays with the increase of the pressure may attribute to the competitive relationship between reactions R332 and R333 in consumption of C_4H_5-n. In the NUI_MF2 model, the rates of these two reactions were updated from Laskin et al.29 by CBS-QB3 energetics and partition functions and a QRRK treatment to account for the pressure dependence.[15] The comparisons for rate constants of reactions R332 and R333 are given in Figure 8 as well as rate constants from other literature sources.[29−32] It is

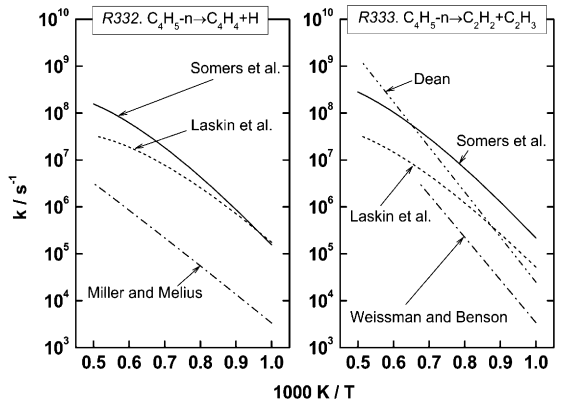

Figure 8. Comparison of reaction rate constants for reaction R332 (C_4H_5-$n \rightarrow C_4H_4 + H$) and reaction R333 (C_4H_5-$n \rightarrow C_2H_2 + C_2H_3$) at a pressure of 10 atm.

noted that the rate constants were given in reverse direction by Laskin et al.;[29] the reverse rate constants were calculated on the basis of the reaction equilibrium constant. Table 2 lists the rate constants and are illustrated in Figure 8 for these two reactions at 10 atm. Apparently, the rate constants of reactions R332 and R333 show large discrepancies among different sources at a pressure of 10 atm. The rate constants updated by Somers et al.[15] generally show the largest rate under the concerned temperature range from 1000 to 2000 K. To achieve a better prediction of the measured ignition delays, a simple attempt that the rate of constants of reactions R332 and R333 are multiplied by a constant factor artificially based on the sensitivity analysis was made. With regard to the rates of reactions R332 and R333, Somers et al.[15] considered the pressure dependence covering the pressure range of 0.001−1000 atm (specified at pressures of 0.001, 1, 2, 5, 10, 100, and 1000 atm) in the 2-MF model NUI_MF2. Because NUI_MF2 gives good ignition delay prediction at 1.25 bar and underpredicts the ignition delays at 4.25 and 10.65 bar, only the modification on the rate constants is performed for the rates higher than a pressure of 2.0 atm. Thus, a factor of 4 was chosen to multiply or divide the pre-exponent *A* factor of reaction R332 or R333, respectively. Obviously, the predicted ignition delays are improved in comparison to the NUI_MF2 model, as shown in Figure 9, after the perturbation on rate constants of reaction R332 or R333. It is also noted that the calculated ignition delays at 1.25 bar are still kept unchanged. Moreover, the modified rate of reaction R332 exhibits better ignition delay prediction performance than that modified on the rate of reaction R333.

3.6. Reaction Pathway Analysis. In this section, the reaction pathway of 2-MF under elevated pressure based on NUI_MF2 was analyzed, as well as the models with quadrupling the rate constant of reaction R332 and quartering the rate constant of reaction R333. As shown in Figure 10, the pathway analysis was carried out at 1330 K and 10.65 bar, which is the same condition as that of the sensitivity analysis. Here, the analyses provide a snapshot of the reaction pathway at 20% fuel consumption conditions.

For reaction pathway analysis based on NUI_MF2, as shown in Figure 10a, there are four types of reactions (i.e., H-abstraction, H-addition, H-transfer, and OH-addition reactions) involved in fuel consumption. Because the reaction flux going through the H-transfer and OH-addition reactions attribute very little fuel consumption, their downstream pathways were not given here in detail. Concerning the H-abstraction reactions, 2-

dx.doi.org/10.1021/ef401809y | Energy Fuels 2013, 27, 7809−7816

Table 2. Rate Coefficients in Form of $k = AT^n \exp(-E/RT)$ for Reaction R332 (C_4H_5-$n \rightarrow C_4H_4 + H$) and Reaction R333 (C_4H_5-$n \rightarrow C_2H_2 + C_2H_3$)

reaction		A (s^{-1})	n	E (cal mol^{-1})	reference
R332. C_4H_5-$n \rightarrow C_4H_4 + H$		2.030×10^{49}	−10.58	5.660×10^4	15
		4.337×10^{48}	−10.78	5.054×10^4	29[a]
	high	1.000×10^{14}	0.00	3.700×10^4	30
	low	1.000×10^{14}[b]	0.00	3.000×10^4	
R333. C_4H_5-$n \rightarrow C_2H_2 + C_2H_3$		1.220×10^{48}	−10.14	5.638×10^4	15
		7.802×10^{46}	−10.14	5.376×10^4	29[a]
		1.000×10^{14}	0.00	4.392×10^4	31[c]
		4.863×10^{13}	0.30	4.233×10^4	32

[a]Calculated using the reaction equilibrium constant. [b]The unit is cm^3 mol^{-1} s^{-1}. [c]High-pressure limit.

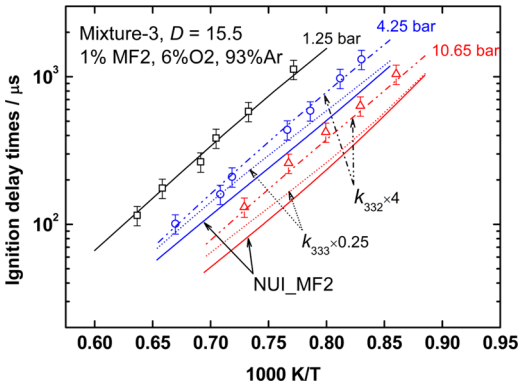

Figure 9. Comparison between measured ignition delays for mixture 3 and model prediction for different rate constants of reactions R332 and R333 at elevated pressure (black square, 1.25 bar; blue circle, 4.25 bar; and red triangle, 10.65 bar).

MF is majorly consumed by free radicals to yield the mf22j fuel radical because the bond dissociation energy of the C−H bond at the methyl side is relatively lower than that at the furan ring.[15] Overall, 47.3, 2.1, 2.1, and 2.1% of fuel convert to fuel radicals at the site of the methyl side, C(3), C(4), and C(5), respectively. It is noted that most of the mf22j fuel radical will ultimately convert to the C_4H_5-n radical at elevated pressure, the same behavior as Somers et al.,[15] at atmosphere pressure. Subsequently, 27.3 and 42.8% of C_4H_5-n undergoes β-scission reactions R332 and R333, respectively. The rest of the C_4H_5-n radical reacts with molecular oxygen through reactions R334−R336. On the other hand, there are four available H-addition sites on the furan ring for molecular 2-MF. However, through the reaction pathway analysis, only the H addition on C(2) and C(5) sites is dominated, although 0.4% of fuel is consumed by H addition on C(3) and C(4) sites. H addition at the C(2) site consumes 19.9% of fuel, with 10.8% of this yielding the methyl radical and furan and 9.1% converting to C−C−C═C* and carbon monoxide. Meanwhile, H addition at the C(5) site consumes 22.1% of fuel, which subsequently forms vinyl ketene and methyl radical (19.9%) and C−C*−C═C and carbon monoxide (1.8%).

As mentioned in the previous section, an artificial perturbation on the pre-exponential A factor can give better agreement with the ignition delays at elevated pressure. Here, we examine the reaction pathway considering these individual two perturbations on NUI_MF2. First, in the case of quadrupling the pre-exponential A factor of reaction R332, as shown in Figure 10b, it can be seen that the fuel consumption flux is similar to that of the NUI_MF2 model. However, the branching ratio of β-scission reactions for C_4H_5-n differs from that of NUI_MF2. When increasing the rate constant of reaction R332, 59.4 and 23.4% of C_4H_5-n undergo β-scission reactions R332 and R333 to yield $C_4H_4 + H$ and $C_2H_2 + C_2H_3$, respectively. Second, in the case of quartering the pre-exponential A factor of reaction R333, as shown in Figure 10c, one can observes that the fuel reaction flux is similar to that depicted in panels a and b of Figure 10. Only the difference with NUI_MF2 is found in β-scission reactions of the C_4H_5-n radical. A total of 40.1 and 15.7% of C_4H_5-n goes through β-scission reactions R332 and R333 to yield $C_4H_4 + H$ and $C_2H_2 + C_2H_3$, respectively. In this sense, a perturbation on the rate of R332 or R333 can affect the branching ratio of β-scission reactions of the C_4H_5-n radical and has little effect on the primary reaction flux of 2-MF at elevated pressure. Moreover, the perturbation made on reaction R332 or R333 achieves better predictions for the measured ignition delays in this study, as shown in Figure 9, leading to the probable products of the C_4H_5-n radical β-scission reaction as being C_4H_4 and a H atom. This is in accordance with the analysis on bond dissociation energy of C_4H_5-n in ref 28. Nevertheless, as described in Figure 8, the rate constants for the C_4H_5-n β-scission reaction from different studies have large discrepancies. The perturbations made above, with the constant factor of 4 modified for the pre-exponential A factor, may be accepted or be within the uncertainty of calculation based on QBS-CB3, and a further study on high-level *ab initio* calculation is appreciated.

4. CONCLUSION

Shock-tube ignition delays were experimentally measured for 2-MF over equivalence ratios of 0.25−2.0, average pressures of 1.25−10.65 bar, temperatures of 1120−1700 K, and oxygen concentrations up to 20%. The main conclusions are summarized as follows: (1) For a given dilution ratio, there exists a crossover in the dependence of ignition delay upon the equivalence ratio when the temperature is increased. This crossing point shifts to the higher temperature as the pressure increases. (2) The NUI_MF2 model yields good predictions for 2-MF at lower pressures (1.25 bar) but underpredicts at elevated pressure. The dominate reactions in the 2-MF ignition were identified through sensitivity analysis based on the NUI_MF2 model. Improvement on ignition delay prediction is achieved by perturbing the rate constants of reaction R332 (C_4H_5-$n \rightarrow C_4H_4 + H$) or reaction R333 (C_4H_5-$n \rightarrow C_2H_2 + C_2H_3$) at elevated pressure. (3) 2-MF majorly undergoes H-abstraction and H-addition reactions at elevated pressure. Perturbation on reaction R332 or R333 does not affect the fuel consumption flux; the only difference is observed in the branching ratio of β-scission for the C_4H_5-n radical. (4) Considering large sensitivity by the reactions involving the C_4H_5-n radical and large discrepancies for the existing rate constant at elevated pressure, a high-level *ab initio* calculation is appreciated.

dx.doi.org/10.1021/ef401809y | *Energy Fuels* 2013, 27, 7809−7816

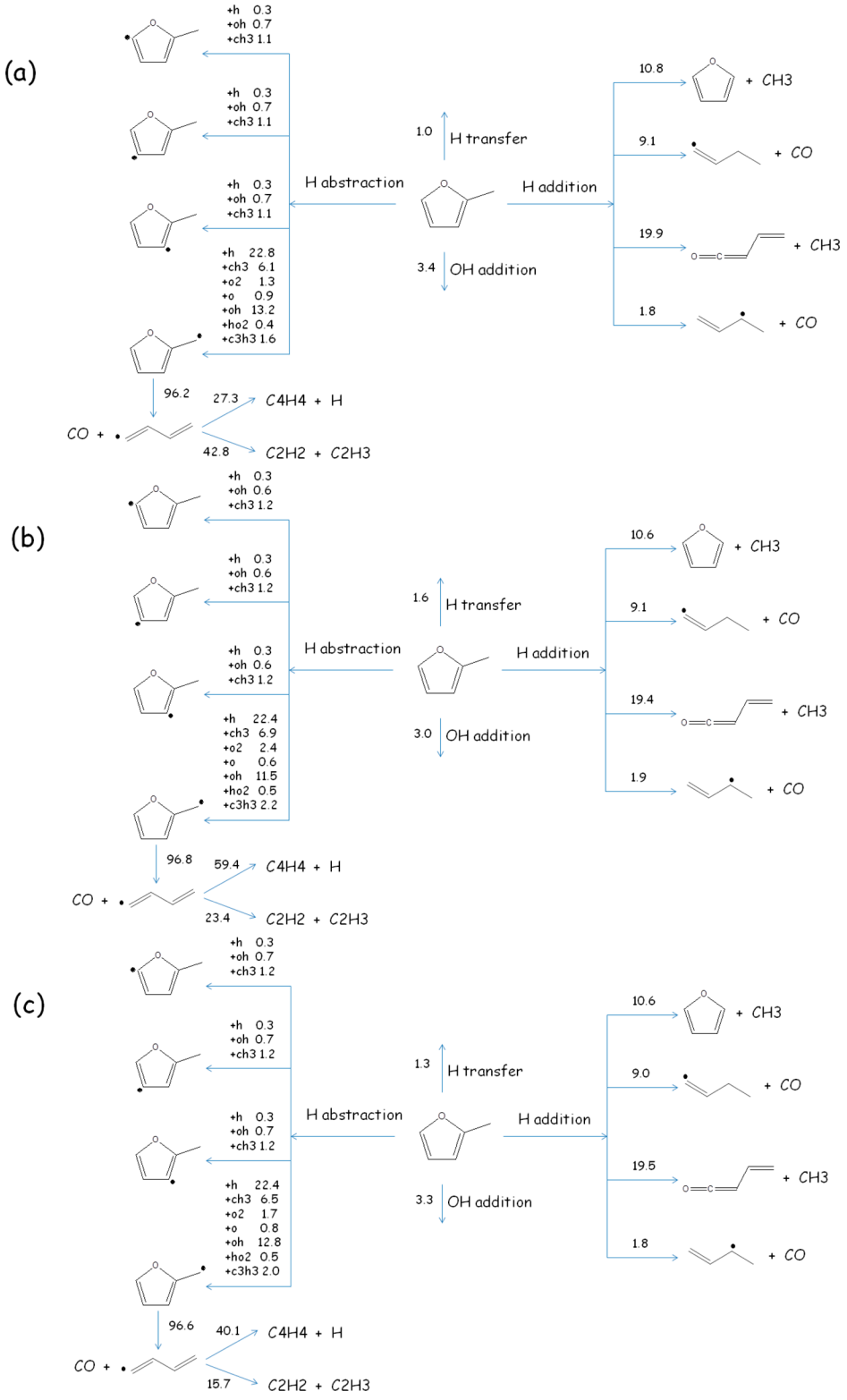

Figure 10. Primary reaction pathway analysis of mixture 3 at 1330 K and 10.65 bar and 20% fuel consumption: (a) NUI_MF2, (b) quadrupling the *A* factor of reaction R332, and (c) quartering the *A* factor of reaction R333.

■ ASSOCIATED CONTENT

Supporting Information

All experimental data of ignition delay times of 2-MF. This material is available free of charge via the Internet at http://pubs.acs.org.

■ AUTHOR INFORMATION

Corresponding Authors

*Telephone: 0086-29-82665075. Fax: 0086-29-82668789. E-mail: chenglongtang@mail.xjtu.edu.cn.
*Telephone: 0086-29-82665075. Fax: 0086-29-82668789. E-mail: zhhuang@mail.xjtu.edu.cn.

dx.doi.org/10.1021/ef401809y | *Energy Fuels* 2013, 27, 7809−7816

Notes

The authors declare no competing financial interest.

■ ACKNOWLEDGMENTS

This study was supported by the National Natural Science Foundation of China (51136005 and 51121092) and the National Basic Research Program (2013CB228406). The authors appreciate the helpful discussions with Dr. P. Zhang.

■ REFERENCES

(1) Kohse-Höinghaus, K.; Oßwald, P.; Cool, T. A.; Kasper, T.; Hansen, N.; Qi, F.; Westbrook, C. K.; Westmoreland, P. R. Biofuel combustion chemistry: From ethanol to biodiesel. *Angew. Chem., Int. Ed.* **2010**, *49*, 3572−3597.

(2) Tran, L. S.; Sirjean, B.; Glaude, P. A.; Fournet, R.; Battin-Leclerc, F. Progress in detailed kinetic modeling of the combustion of oxygenated components of biofuels. *Energy* **2012**, *43*, 4−18.

(3) Roman-Leshkov, Y.; Barrett, C. J.; Liu, Z. Y.; Dumesic, J. A. Production of dimethylfuran for liquid fuels from biomass-derived carbohydrates. *Nature* **2007**, *447*, 982−985.

(4) Geilen, F. M. A.; vom Stein, T.; Engendahl, B.; Winterle, S.; Liauw, M. A.; Klankermayer, J.; Leitner, W. Highly selective decarbonylation of 5-(hydroxymethyl)furfural in the presence of compressed carbon dioxide. *Angew. Chem., Int. Ed.* **2011**, *50*, 6831−6834.

(5) Lifshitz, A.; Tamburu, C.; Shashua, R. Thermal decomposition of 2,5-dimethylfuran. Experimental results and computer modeling. *J. Phys. Chem. A* **1998**, *102*, 10655−10670.

(6) Wu, X. S.; Huang, Z. H.; Yuan, T.; Zhang, K. W.; Wei, L. X. Identification of combustion intermediates in a low-pressure premixed laminar 2,5-dimethylfuran/oxygen/argon flame with tunable synchrotron photoionization. *Combust. Flame* **2009**, *156*, 1365−1376.

(7) Friese, P.; Simmie, J. M.; Olzmann, M. The reaction of 2,5-dimethylfuran with hydrogen atoms—An experimental and theoretical study. *Proc. Combust. Inst.* **2013**, *34*, 233−239.

(8) Sirjean, B.; Fournet, R. Theoretical study of the reaction 2,5-dimethylfuran plus H-products. *Proc. Combust. Inst.* **2013**, *34*, 241−249.

(9) Thewes, M.; Muether, M.; Pischinger, S.; Budde, M.; Brunn, A.; Sehr, A.; Adomeit, P.; Klankermayer, J. Analysis of the impact of 2-methylfuran on mixture formation and combustion in a direct-injection spark-ignition engine. *Energy Fuels* **2011**, *25*, 5549−5561.

(10) Ohtomo, M.; Nishikawa, K.; Suzuoki, T.; Miyagawa, H.; Koike, M. Auto-ignition characteristics of biofuel blends for SI engines. *SAE [Tech. Pap.]* **2011**, DOI: 10.4271/2011-01-1989.

(11) Wang, C. M.; Xu, H. M.; Daniel, R.; Ghafourian, A.; Herreros, J. M.; Shuai, S. J.; Ma, X. Combustion characteristics and emissions of 2-methylfuran compared to 2,5-dimethylfuran, gasoline and ethanol in a DISI engine. *Fuel* **2013**, *103*, 200−211.

(12) Grela, M. A.; Amorebieta, V. T.; Colussi, A. J. Very low-pressure pyrolysis of furan, 2-methylfuran, and 2,5-dimethylfuran—The stability of the furan ring. *J. Phys. Chem.* **1985**, *89*, 38−41.

(13) Lifshitz, A.; Bidani, M.; Bidani, S. Thermal-reactions of cyclic ethers at high-temperatures 3. Pyrolysis of furan behind reflected shocks. *J. Phys. Chem.* **1986**, *90*, 5373−5377.

(14) Lifshitz, A.; Tamburu, C.; Shashua, R. Decomposition of 2-methylfuran. Experimental and modeling study. *J. Phys. Chem. A* **1997**, *101*, 1018−1029.

(15) Somers, K. P.; Simmie, J. M.; Gillespie, F.; Burke, U.; Connolly, J.; Metcalfe, W. K.; Battin-Leclerc, F.; Dirrenberger, P.; Herbinet, O.; Glaude, P. A.; Curran, H. J. A high temperature and atmospheric pressure experimental and detailed chemical kinetic modelling study of 2-methyl furan oxidation. *Proc. Combust. Inst.* **2013**, *34*, 225−232.

(16) Wei, L.; Li, Z.; Tong, L.; Wang, Z.; Jin, H.; Yao, M.; Zheng, Z.; Wang, C.; Xu, H. Primary combustion intermediates in lean and rich low-pressure premixed laminar 2-methylfuran/oxygen/argon flames. *Energy Fuels* **2012**, *26*, 6651−6660.

(17) Tran, L. S.; Togbé, C.; Liu, D.; Felsmann, D.; Oßwald, P.; Glaude, P. A.; Fournet, R.; Sirjean, B.; Battin-Leclerc, F.; Kohse-Höinghaus, K. Combustion chemistry and flame structure of furan group biofuels using molecular-beam mass spectrometry and gas chromatography—Part II: 2-Methylfuran. *Combust. Flame* **2013**, DOI: 10.1016/j.combustflame.2013.05.027.

(18) Wei, L.; Tang, C.; Man, X.; Jiang, X.; Huang, Z. High-temperature ignition delay times and kinetic study of furan. *Energy Fuels* **2012**, *26*, 2075−2081.

(19) Morley, C. *Gaseq: A Chemical Equilibrium Program for Windows*; http://www.c.morley.dsl.pipex.com/.

(20) Tian, Z.; Yuan, T.; Fournet, R.; Glaude, P. A.; Sirjean, B.; Battin-Leclerc, F.; Zhang, K.; Qi, F. An experimental and kinetic investigation of premixed furan/oxygen/argon flames. *Combust. Flame* **2011**, *158*, 756−773.

(21) Sendt, K.; Bacskay, G. B.; Mackie, J. C. Pyrolysis of furan: Ab initio quantum chemical and kinetic modeling studies. *J. Phys. Chem. A* **2000**, *104*, 1861−1875.

(22) Metcalfe, W. K.; Dooley, S.; Dryer, F. L. Comprehensive detailed chemical kinetic modeling study of toluene oxidation. *Energy Fuels* **2011**, *25*, 4915−4936.

(23) Lutz, A. E.; Kee, R. J.; Miller, J. A. *SENKIN: A Fortran Program for Predicting Homogeneous Gas Phase Chemical Kinetics with Sensitivity Analysis*; Sandia National Laboratories: Livermore, CA, 1988; SAND87-8248.

(24) Kee, R. J.; Rupley, F. M.; Miller, J. A. *CHEMKIN-II: A FORTRAN Chemical Kinetics Package for the Analysis of Gas-Phase Chemical Kinetics*; Sandia National Laboratories: Livermore, CA, 1989; SAND89-8009.

(25) Healy, D.; Donato, N. S.; Aul, C. J.; Petersen, E. L.; Zinner, C. M.; Bourque, G.; Curran, H. J. *n*-Butane: Ignition delay measurements at high pressure and detailed chemical kinetic simulations. *Combust. Flame* **2010**, *157*, 1526−1539.

(26) Healy, D.; Donato, N. S.; Aul, C. J.; Petersen, E. L.; Zinner, C. M.; Bourque, G.; Curran, H. J. Isobutane ignition delay time measurements at high pressure and detailed chemical kinetic simulations. *Combust. Flame* **2010**, *157*, 1540−1551.

(27) Stranic, I.; Chase, D. P.; Harmon, J. T.; Yang, S.; Davidson, D. F.; Hanson, R. K. Shock tube measurements of ignition delay times for the butanol isomers. *Combust. Flame* **2012**, *159*, 516−527.

(28) Law, C. K. *Combustion Physics*; Cambridge University Press: New York, 2006.

(29) Laskin, A.; Wang, H.; Law, C. K. Detailed kinetic modeling of 1,3-butadiene oxidation at high temperatures. *Int. J. Chem. Kinet.* **2000**, *32*, 589−614.

(30) Miller, J. A.; Melius, C. F. Kinetic and thermodynamic issues in the formation of aromatic-compounds in flames of aliphatic fuels. *Combust. Flame* **1992**, *91*, 21−39.

(31) Dean, A. M. Predictions of pressure and temperature effects upon radical addition and recombination reactions. *J. Phys. Chem.* **1985**, *89*, 4600−4608.

(32) Weissman, M. A.; Benson, S. W. Rate parameters for the reactions of C_2H_3 and C_4H_5 with H_2 and C_2H_2. *J. Phys. Chem.* **1988**, *92*, 4080−4084.